Simple way of pinpointing the three-dimensional position of biomarkers in fluorescence microscopy using a through-focus exposure method

Koichiro Kishima

LE Business Development Department, Core Device Development Group, Sony Corporation, 5-1-12 Kitashinagawa Shinagawa-ku, Tokyo 141-0001, Japan
(koichiro.kishima@jp.sony.com)

Received 28 March 2011; revised 7 June 2011; accepted 7 July 2011;
posted 11 July 2011 (Doc. ID 144790); published 29 August 2011

The author proposes a method to identify the three-dimensional positions of fluorescent biomarkers by recording just two images. In the proposed method, the x and y positions of all fluorescent markers are recorded in the first exposure, and the z positions are obtained from a blurred image in the second exposure. The author has verified this method using a specimen with 1 μm deep grooves and applied it to measuring chromatic aberration and the separation between two biological probes in fluorescence *in situ* hybridization cells. The method offers the advantage of greatly reduced data storage requirements. ©2011 Optical Society of America

OCIS codes: 180.2520, 180.6900, 110.4190.

1. Introduction

To analyze specific chromosomes in human cells, fluorescence *in situ* hybridization (FISH) [1,2] is commonly used in diagnosis and drug discovery. FISH analysis is used to observe a fluorescent probe that is hybridized to a specific chromosome with a fluorescence microscope. In current cancer research, three-dimensional (3D) analysis of specific chromosomes and proteins in cells is becoming more important for understanding signal transduction mechanisms, drug sensitivity, and in activating mutations [3]. The intrachromosomal recombination frequency was shown to be inversely proportional to the distance between two recombination sites by applying a Cre-mediated chromosomal recombination system using fluorescent proteins and different site-specific recombinases [4]. To perform 3D analysis of chromosomes and proteins in cells, it is necessary to identify the 3D positions of fluorescent probes.

0003-6935/11/254989-09$15.00/0

In the research field of fluorescence microscopy, the optical diffraction limit has been overcome using new concepts such as stimulated emission depletion [5,6], structured illumination microscopy [7], photoactivated localization microscopy (PALM) [8], and stochastic optical reconstruction microscopy (STORM) [9]. The PALM and STORM methods employ photoactivated fluorescent probes to achieve super-resolution imaging of spatial differences in dense populations of molecules. Single-molecule localization is achieved by superimposing the point-spread function of a widefield fluorescence microscope onto a wireframe representation of the pixel array of a digital camera. Research into super-resolution imaging in fluorescence microscopy is still being actively pursued, and there have been reports of live-cell imaging [10] and 3D imaging [11,12] being achieved. In addition to super-resolution imaging, 3D fluorescence microscopy has also received considerable attention recently, with reports on the use of a spatial light modulator [13,14], a cylindrical lens [15], and a quadratically distorted grating [16]. Although these methods are convenient for acquiring multiple images at

different focal positions simultaneously, the observation area decreases in inverse proportion to the number of focal layers because a different part of the imaging device area is assigned to each layer.

In the semiconductor field, fluorescence microscopy can also be applied to nondestructive defect inspection of silicon substrates. Navin *et al.* reported the use of fluorescence microscopy to identify the position of defects at depths from 1 to 3 μm from the surface of a silicon substrate by detecting a photoluminescence signal during illumination with 532 nm light [17]. Recently, electronic and photonic integrated circuits [18,19] have received considerable attention as high-speed next-generation signal processing devices. The use of electronic and photonic double-layer substrates is a promising approach since it allows the optimum use of the silicon surface [20]. However, there is a risk of defect introduction into the substrate due to previously fabricated optical circuits. Because optical circuits are less sensitive to defects than electronic circuits, defects at depths of about 1 μm or more from the surface have an almost negligible impact on the device, whereas those within the top 0.5 μm can cause serious problems [21]. Therefore, a nondestructive inspection method which can identify the depth of defects is required.

When the region of interest in a specimen is limited, locating it can be time-consuming using current 3D fluorescence microscopy techniques because of the reduced observation area. An extended depth of field method employing a phase mask have been shown to be effective in identifying the target for observation because the depth of focus is extended [22]. However, it is difficult to extend the depth of focus to about 5 μm, which is the normal thickness of a biological sample, without a degradation of the optical quality. In addition, this method does not support 3D imaging.

As a result, in many cases, a method of recording multiple images at different focal positions using a widefield microscope, which is a traditional method, is used to find the target area for 3D fluorescence microscopy observations.

On the other hand, in the field of computational photography, there has recently been remarkable progress in handling blurred images [23–25]. Flexible depth of field photography [25] can create focused images of objects at different focal positions by analyzing blurred pictures taken by an imaging device moving in the focal direction during exposure.

The author has proposed a method to determine the depth of fluorescent markers by analyzing blurred images that contain projected depth information. This method requires only two exposures using a conventional widefield fluorescence microscope, and it has sufficient precision to identify the 3D position of fluorescent probes. The accuracy of the depth measurements has been confirmed using a specimen in which fluorescent beads are placed both on the top and at the bottom of 1 μm deep grooves fabricated on a fused silica substrate. The application of this method to measure the chromatic aberration of the microscope optics and the true separation between different color fluorescent bio probes in FISH cells is demonstrated. Because there is no need to use photoactivated protein, this method is applicable to all kinds of fluorescent markers in addition to nondestructive defect inspection of silicon substrates.

2. Traditional Method for Obtaining Depth Information in Fluorescence Microscopy

Figure 1 shows the procedure for identifying the 3D position of fluorescent markers using the traditional method. Multiple images are recorded at different focal positions (z positions) at fine step intervals, as shown in Fig. 1(a). Next, the brightness of the fluorescent markers is plotted against the z position corresponding to each image, as shown in Fig. 1(b). The actual z position of each marker can then be determined from the peak of the brightness curves.

The analysis can be carried out by computer using a simple algorithm to automatically determine the 3D position of fluorescent markers. However, if the region of interest is limited, computer analysis requires a large amount of memory to handle the high volume of data associated with the multiple images. For example, if the sample dimensions are 15 mm × 15 mm × 5 μm and the pixel resolution is 0.15 μm /pixel, the data size is 600 GB in Tiff format and 30 GB in JPEG format even if the focal interval between images is 0.25 μm. This corresponds to about 130 MB/mm^2 in JPEG format. Since the area of a current 300 mm silicon substrate is about 70000 mm^2, about 9 TB of storage space is required per wafer, even if image files are compressed to JPEG format. Therefore, a method with smaller storage requirements is desirable. The data size cannot be reduced by applying current 3D imaging techniques

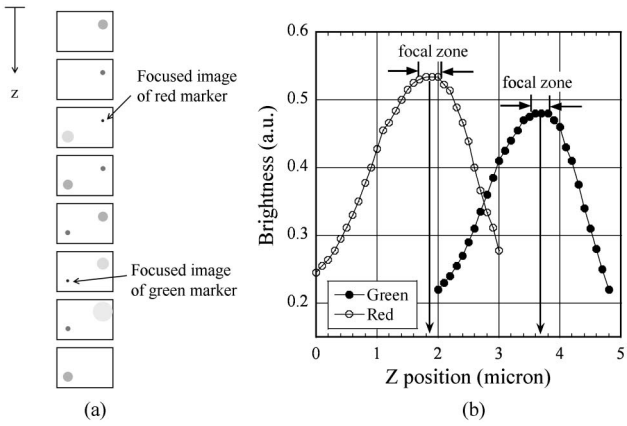

Fig. 1. Procedure for finding the z positions of the fluorescent markers in the traditional method. (a) First step: capturing multiple images with fine intervals in the z direction. A red and a green fluorescent marker are seen in the right and left portion of the image, respectively. They have different focus positions. (b) Second step: plotting the peak brightness data for each fluorescence marker, determining the focal depth, identifying the position of the markers.

[13–16] because the image quality is the same as that for the traditional method.

3. Proposed Through-Focus Exposure Method

In the through-focus exposure method, the specimen is moved in the x, y, and z directions during exposures, and the positions of the fluorescent markers are identified by a two-step process. Figure 2 shows a schematic illustration of a 3D structure for analysis. Marker A emits green fluorescent light and marker B emits red light. The z positions of markers A and B are z_A and z_B, respectively. In addition, z_A is at the midpoint between z_{start} and z_{end}, whereas z_B is closer to z_{end}.

The first step involves moving the microscope stage with the specimen in the z direction only. This movement can be described by Eq. (1). The focal plane of the microscope moves from z_{start} to z_{end} at constant velocity during the exposure time t. At the beginning of exposure ($t = 0$), the focal plane is at z_{start} and at the end of exposure ($t = t_{\text{ex}}$) it is at z_{end}. The x and y positions are fixed during exposure, as expressed by Eqs. (2) and (3).

$$z(t) = z_{\text{start}} + (z_{\text{end}} - z_{\text{start}})\frac{t}{t_{\text{ex}}} \tag{1}$$

$$x = x_0 \tag{2}$$

$$y = y_0. \tag{3}$$

Figure 3(a) shows a schematic diagram illustrating the change in the image of fluorescent marker A with time t during exposure. At the beginning of the exposure ($t = 0$), the focal plane is at z_{start} and the image is defocused. When $t = 1/2t_{\text{ex}}$, the focal plane of the microscope is at $(z_{\text{end}} + z_{\text{start}})/2$ where marker A exists and the image is in focus. At this moment, the size of the image is at a minimum and its brightness is at a maximum. At the end of exposure ($t = t_{\text{ex}}$), the image plane is at z_{end} and the image of marker A is again defocused.

Figure 3(b) shows an illustration of the recorded image. Because both marker A and B are between z_{start} and z_{end}, at some point during the exposure each will be in focus. Because the stage was not moved in the x or y directions during exposure, the x and y positions of markers A and B can be identified in the recorded image.

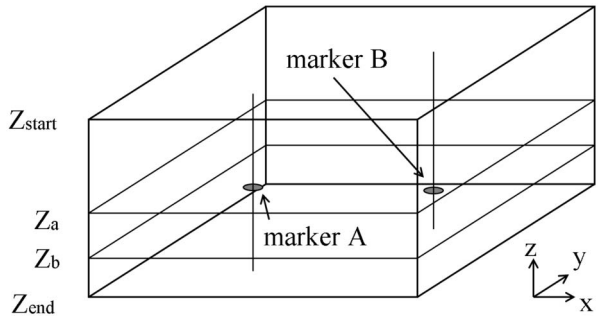

Fig. 2. 3D structure to explain the proposed method. Marker A is on the z_A plane and marker B is on the z_B plane.

In the second step of the process, information on the z position of the fluorescent markers is obtained from blurred images produced by moving the microscope stage in the x, y, and z directions during exposure, as expressed by Eqs. (4)–(6). The z axis movement is the same as in the first step, whereas the x and y movements describe a circular path with a radius of L. The center of the circle is the point (x_0, y_0), at which the previous exposure was performed:

$$z(t) = z_{\text{start}} + (z_{\text{end}} - z_{\text{start}})\frac{t}{t_{\text{ex}}} \tag{4}$$

$$x(t) = x_0 + L \times \cos\left(\pi\frac{t}{t_{\text{ex}}}\right) \tag{5}$$

$$y(t) = y_0 + L \times \sin\left(\pi\frac{t}{t_{\text{ex}}}\right). \tag{6}$$

Figure 4(a) shows a schematic diagram illustrating the change in the image of fluorescent marker A with time t during exposure. At the beginning of exposure ($t = 0$), the focal plane is at z_{start} and the image of marker A is defocused. As t increases, the image of the marker on the imaging device follows a circular path with a radius of $L \times M$, where M is the microscope magnification. When $t = 1/2t_{\text{ex}}$, the focal plane of the microscope is at $(z_{\text{end}} + z_{\text{start}})/2$ where marker

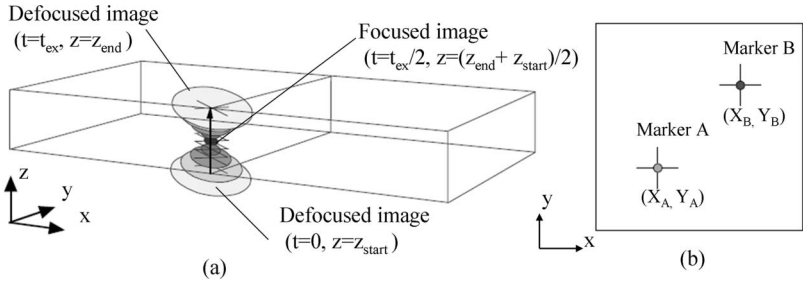

Fig. 3. First step: identifying the xy position of markers using through-focus exposure. (a) Image of fluorescent marker A on imaging device as a function of time t during exposure. (b) Image of markers A and B recorded by through-focus exposure. xy positions of marker A and B are identified as (X_A, Y_A) and (X_B, Y_B), respectively.

A exists. The marker image is then in focus and has a minimum size and maximum brightness. At the end of exposure ($t = t_{ex}$), the focal plane is at z_{end}, and the image is again defocused.

Figure 4(b) shows a schematic of the final recorded image, with the blurred circular arcs associated with markers A and B, whose centers correspond to the positions of these markers in Fig. 3(b). The points on the arcs where the biomarkers are in focus can be identified as the points of maximum brightness. Lines A and B can then be drawn between the center points and the focus points, as shown in the figure. The angles θ_A and θ_B are indicators of the elapsed time when the focal plane was on marker A and marker B, respectively, which directly corresponds to the z position of the markers. In Fig. 4(b), lines A and B are drawn merely to illustrate the relationship between the angles and the z position; in actual measurements there is no need to draw these lines.

If the purpose of the observation is simply to measure the separation between two fluorescent markers, the x and y components can be obtained from Fig. 3(b) and the z component by measuring the difference between the angles in Fig. 4(b).

4. Experimental Verification of Proposed Method

A. Experimental Setup and Sample Preparation

The experimental setup is shown in Fig. 5. The fluorescence microscope used was a widefield system (Axio Imager Z1, Carl Zeiss). A piezo-type xy stage (P-628K001, Physik Instrumente) and piezo-type z stage (P-622.ZCL, Physik Instrumente) is placed on the microscope stage in order to move the specimen during exposure. The xy stage is controlled by an xy stage controller (E-710.4CL, Physik Instrumente) and the z stage by a z stage controller (E-661CP, Physik Instrumente). The z stage position is set using a function generator. Both stages are controlled by a closed loop servo system. The position of the z stage is monitored using a digital oscilloscope (TDS220, Tektronix). A digital SLR camera (Alpha 900, Sony) is connected to the fluorescence microscope using a 2.5× adapter lens (Carl Zeiss). The Alpha 900 has a full-size CMOS color image sensor (24.81 megapixels) with a pixel pitch of 5.94 μm. The

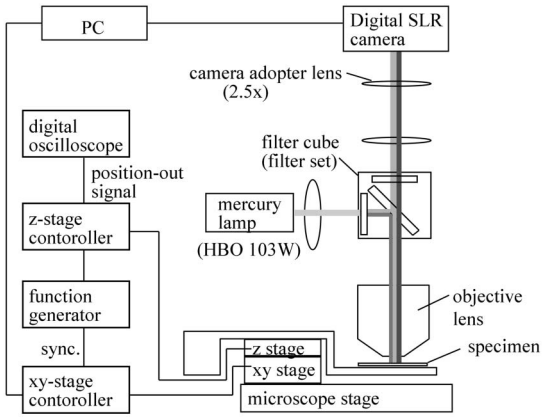

Fig. 5. Experimental setup. Piezo-type stages xy and z stages are placed on the stage of FOV-type fluorescent microscope; Axio Imager Z1 (Carl Zeiss). Color digital SLR camera is used.

digital camera and xy stage controller are directly controlled by a PC.

By applying a sine and cosine function (amplitude 5 μm, frequency 0.2 Hz) to the x and y inputs of the xy stage, respectively, the stage is made to follow a circular path with a radius of 5 μm and an angular velocity of 72 deg/s. Either a 20× objective lens (Plan-APOCHROMAT 20×/0.8, Carl Zeiss) and a 40× objective lens (EC Plan-NEOFLUAR 40×/0.75, Carl Zeiss) are used in the experiments. Since the image sensor has dimensions of 36.2 mm × 24.1 mm and a 2.5× adopter lens is used, the image capturing area with the 20× and 40× objective lenses is 724 μm × 482 μm and 362 μm × 241 μm, respectively. In addition, due to the circular motion of the xy stage, the entire boundary of the image capturing area is reduced by 5 μm, so the effective image sizes with the 20× and 40× objective lenses are 714 μm × 472 μm and 352 μm × 231 μm, respectively.

The speed of the z stage is set to 3 μm/s and the exposure time is 4 s for both the first and the second exposure. Therefore, the z stage moves by a total of 12 μm during exposures. Between the first and the second exposure, the XY stage moves 5 μm in order to set a center position of circular movement to the position of the first exposure. However the second exposure time is 4 s and traveling angle is 288 deg during exposure. The stage has started to move on the full circle before the second exposure in order to have

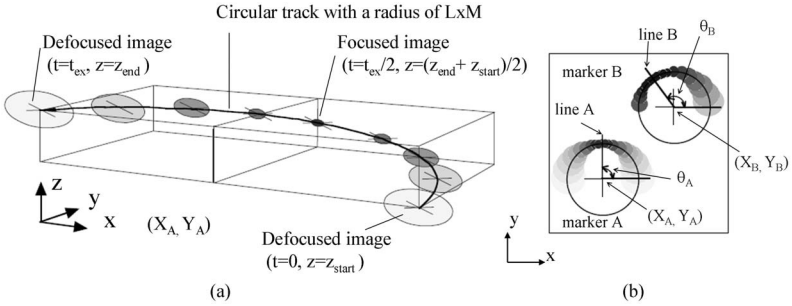

Fig. 4. Second step: identifying the z position of markers from blurred image. (a) Image of fluorescent marker A on imaging device as a function of time t during exposure. (b) Final blurred images of markers A and B.

settling time of 1 s. The total consuming time of this method is about 12 s from the start of the stage movement of the first exposure to the end of the second exposure. In other words, an acquisition time of pinpointing data for all markers in the captured area of 714 μm × 472 μm or 352 μm × 231 μm is 12 s. Although the resolution of the servo systems for both the xy and z stages is 10 nm, the precision in the z direction is only about 0.05 μm due to the presence of vibrations at about 200 kHz.

The specimen used for validation of this method is shown in Fig. 6. It consists of a fused silica substrate with a groove structure produced by reactive ion etching. The groove depth was determined to be 1 μm using a surface profiler (P10, KLA Tencor). Green fluorescent beads with diameters of 0.3 μm (Fluoromax G300, Thermo Fisher Scientific) are placed randomly on the substrate and covered by a 0.17 mm thick cover glass for microscopy observations.

Figure 7 shows images of the fluorescent markers on the specimen taken using the proposed method with 20×/0.8 objective lens. The images are filtered using filter set No. 38 (Carl Zeiss; emission wavelength 525 nm). Figures 7(a) and 7(b) correspond to the two steps described in Section 3 to determine the xy and z positions, respectively. The arrow in Fig. 7(b) shows the image movement direction as the z stage moves closer to the objective lens. The effective NA of objective lens in the first exposure was evaluated by using Fourier optics [26]. The width at the brightness level of $1/e^2$ of the image of a point source in the first exposure with NA 0.8 objective lens is same with the width of focused image with NA 0.62 objective lens. As can be seen from Fig. 7(a), there is sufficient contrast to easily identify the center positions of the marker images.

B. Results of Verification Experiment

Figure 8 shows the process for determining the z position of the fluorescent markers from the blurred image. Based on Fourier optics, theoretical images were calculated for a monochromatic point source at a given wavelength and a defocus value from 3 to −3 μm [26]. The magnification is defined as the ratio of the numerical apertures of the objective and imaging lens. The final theoretical blurred image was produced by placing each image obtained above at the appropriate position based on the movement of the stage. This composite image was then rotated at 1 degree intervals to produce a total of 360 images for comparison with the experimentally obtained image. MATLAB (Mathworks) was used to calculate the correlation between the cropped experimental image and each of the 360 calculated images in order to obtain the appropriate value of the angle θ (see Fig. 4(b)). The total calculation time was less than 1 s on a standard Windows XP machine (Optiplex 745, Dell Inc.) for image sizes of 100 × 100 and 121 × 121 for the cropped experimental image and theoretical images, respectively.

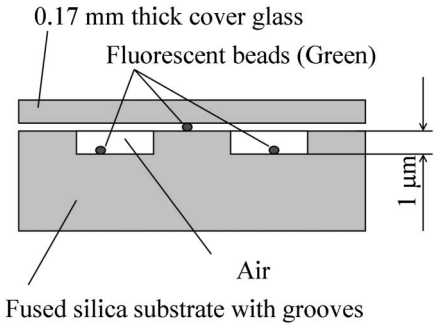

Fig. 6. Specimen for verification of the proposed method.

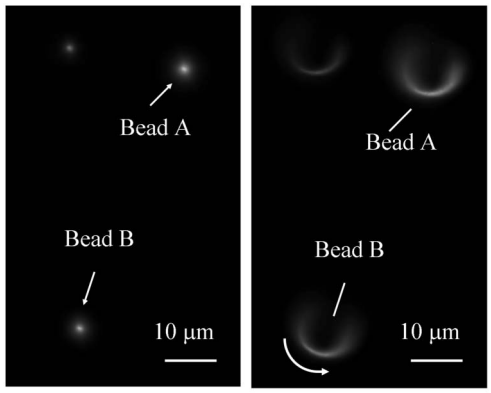

Fig. 7. Images of fluorescent beads on specimen. (a) Image the first step exposure. The z stage was moved during exposure. (b) Image by the second step exposure. The xy stage and z stage were synchronously moved.

Figure 9 shows the localization results for beads A and B on the specimen. The vertical axis is the normalized correlation coefficient between the blurred images of beads A and B in Fig. 7(b) and the theoretical images. The horizontal axis is the image file number of the theoretical images that directly indicates the angle of the images. As can be seen, there is a 25 degree difference between the maxima for beads A and B. Because the speed of the z stage was 3 μm/s and the angular velocity of the xy stage was 72 deg /s, this corresponds to a difference of 1.04 μm in the z positions of beads A and B. This value is very close to the actual groove depth of 1 μm. Based on the direction of movement of the xy and z stages, as indicated in Fig. 7(b), we can determine which of the beads is in the groove. The results indicate that bead B is closer to the objective lens than bead A, i.e., bead A is in the groove.

A XY position of the marker is determined by analyzing the centroid of the image. Since the localization process of marker in z direction uses the correlation between the cropped experimental image and theoretical images, the error in XY position is not sensitive to the localization process only if the cropped experimental image is properly cropped. The error margin associated with the localization process is less than 0.1 μm since 1 degree rotation intervals are used for the theoretical images. The

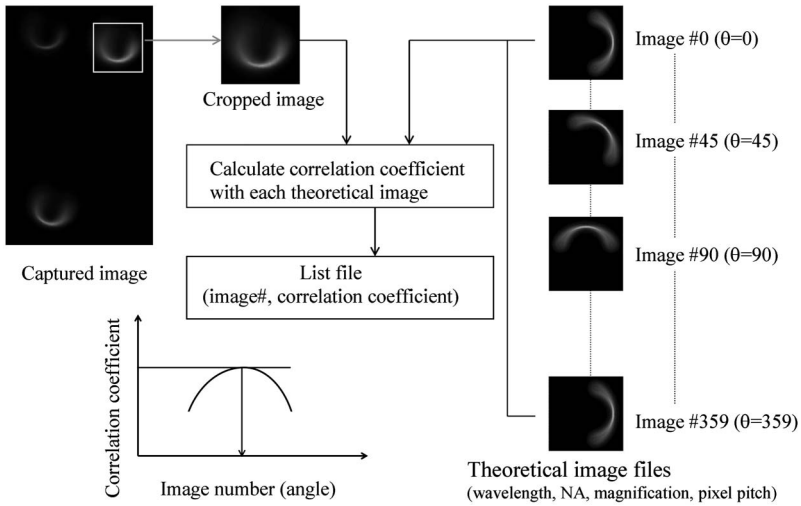

Fig. 8. Localization process of fluorescent marker in z direction.

high-frequency vibration of the z stage described earlier has little effect on the localization process because the stage movement is slow.

These results confirm the effectiveness of the proposed method in pinpointing fluorescent markers three dimensionally. However, since the scanning range in the z direction is $12\,\mu$m in this experiment, localization of fluorescent markers near the bottom or top of this range is more difficult because the theoretical images are calculated for a defocus range of -3 to $+3\,\mu$m. As a result, the effective scanning depth is $6\,\mu$m for a localization error of less than $0.1\,\mu$m. However, this is sufficient for many biological and semiconductor applications. It must again be emphasized that in this method only two captured images are required. By contrast, for a z range of $6\,\mu$m at $0.1\,\mu$m intervals, the traditional method would require 61 exposures.

5. Application to Chromatic Aberration Measurements

Before describing the application of the proposed method to biological cells, the results of measuring chromatic aberration are presented. Figure 10 shows the specimen used for the measurements. Blue, green, and red fluorescent beads with diameters of $0.3\,\mu$m (Fluoro-max B300, G300, and R300; Thermo Fisher Scientific) were placed on a flat glass substrate with a 0.17 mm thick cover glass. Since the z position was the same for all of the beads, the z positions determined using the proposed method should be the same in the absence of chromatic aberration. This implies that any differences due to the color of the beads are a reflection of the degree of chromatic aberration.

Figure 11 shows an image of the second-step exposure to determine the z positions of the fluorescent markers using the 40× objective lens. The filter set used was the triple band fluorescent filter set of 25HE for DAPI (460 nm), FITC (530 nm), and TxRed (630 nm) manufactured by Carl Zeiss. The stage parameters and exposure time were as described in the previous section.

Figure 12 shows the localization results for the blurred images highlighted in Fig. 11, averaged over 5 green and 5 red beads. The theoretical images were calculated based on FITC and TxRed wavelengths for the green and red markers, respectively. A difference of about 10 degrees can be seen between the maxima, corresponding to a z difference of $0.42\,\mu$m

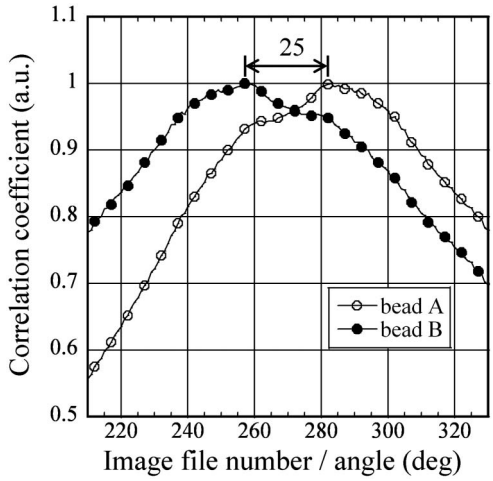

Fig. 9. Results of localization of bead A and B in test specimen.

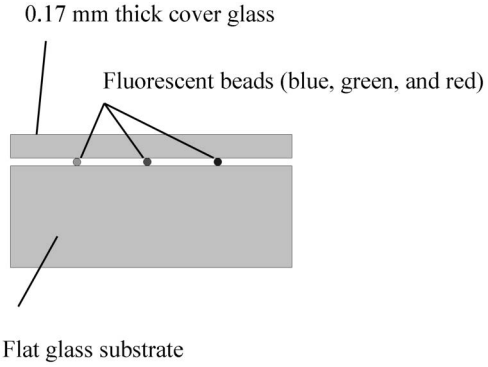

Fig. 10. Specimen for measuring chromatic aberration.

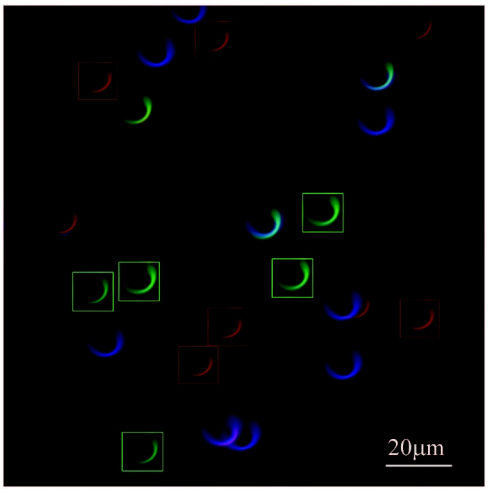

Fig. 11. Images of fluorescent beads of different colors on flat substrate by the second step exposure. The *xy* stage and *z* stage were synchronously moved.

between the FITC and TxRed wavelengths of 530 and 630 nm, respectively. This result indicates that a combination of different colored fluorescent beads placed on a flat substrate, a multiband fluorescent filter set, and a color camera, it is possible to measure the chromatic aberration of the system using the proposed method.

6. Measurement of Distance between FISH Probes in a Biological Cell

A. Sample Preparation and Experimental Conditions

A biological specimen of FISH cells was produced using a UroVysion Bladder Cancer Kit [27], with a cell line of MRC-5 [28]. UroVysion has 4 fluorescent probes that emit different colors for counterstaining cell nuclei. In the present study, attention was focused on two fluorescent probes that emit SpectrumRed and SpectrumGreen, which hybridize to the centromere regions of chromosomes 3 and 7, respectively.

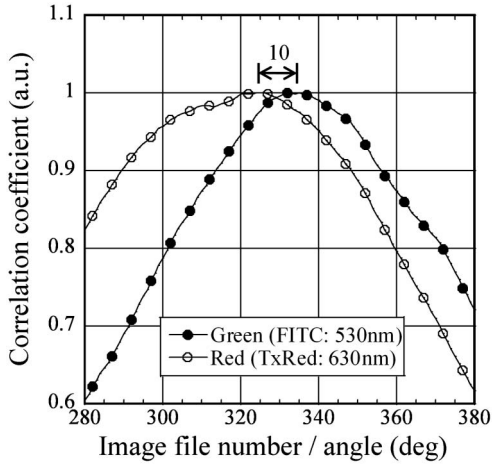

Fig. 12. Results for chromatic aberration measurements. Results of localization of red and green beads on flat substrate.

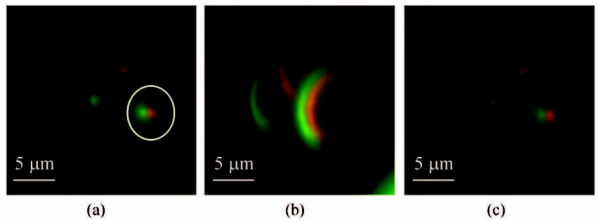

Fig. 13. Images of FISH cells of UroVysion Bladder Cancer Kit. Red color fluorescent probe hybridizes to the centromere regions of chromosomes 3 and green probe hybridizes to the centromere regions of chromosomes 7. (a) Image by the first step exposure. The *z* stage was moved during exposure. (b) Image by the second step exposure. The *xy* stage and *z* stage were synchronously moved. (c) Reference image captured with *xy* and *z* stages fixed.

A dual band filter set (#51006, Chroma Technology Corp.) was used with the 40× objective lens. This filter set is designed for FITC and TxRed and it is also applicable to SpectrumGreen and SpectrumRed. The center wavelengths of the FITC and TxRed emission filters are 530 and 630 nm, respectively, which are the same as the wavelengths used in measuring the chromatic aberration. The stage parameters and exposure time are also as described earlier.

B. Experimental results

Figures 13(a) and 13(b) show first-step and second-step images of the fluorescent probes, respectively, whereas Fig. 13(c) is a fixed-focus image for reference.

Although there are background signals due to counterstaining of the cell nuclei around the FISH markers, the images have sufficient contrast to distinguish the FISH markers even Fig. 13(b). Since the pair of markers of chromosomes 3 and 7 indicated in Fig. 13(a) are in very close proximity, these were chosen for the distance measurement. From Fig. 13(a), the distance between the two markers in the *xy* plane was 0.96 μm. The same result was obtained from Fig. 13(c). Figure 14(a) is a cropped image of the markers chosen for the localization process. Figures 14(b) and 14(c) show the red and green color components of Fig. 14(a), respectively. These are used to identify the positions of chromosomes 3 and 7, respectively.

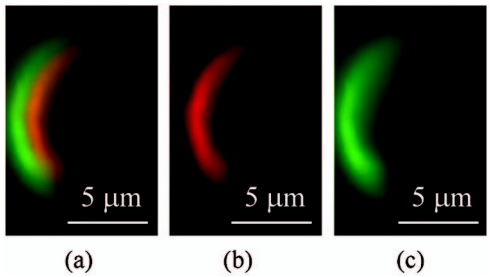

Fig. 14. Cropped blurred images of FISH cells for localization of probe position. (a) Original color (3 color component image) of cropped blurred image (b) Red component of cropped image for localization of probe hybridized to chromosome 3. (c) Green component of cropped image for localization of probe hybridized to chromosome 7.

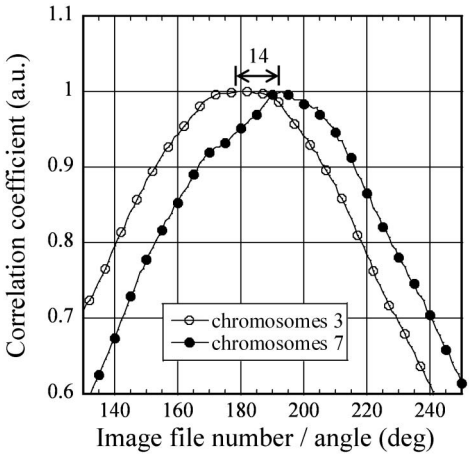

Fig. 15. Results for localization of probes of chromosomes 3 and 7. There is a 14 degree difference between chromosome 3 and 7 before correction for the chromatic aberration shown in Fig. 12.

The localization results are shown in Fig. 15. There is a difference of 14 degrees between the maxima for chromosomes 3 and 7, corresponding to a z difference of $0.58\,\mu$m. Since it is known that a chromatic aberration of $0.42\,\mu$m exists between the FITC and TxRed wavelengths, as shown in Fig. 12, the z distance between chromosomes 3 and 7 is modified to $0.16\,\mu$m. Combining this with the xy value of $0.96\,\mu$m gives a true separation of $0.97\,\mu$m.

7. Conclusion

A method was proposed to measure the 3D positions of fluorescent markers using just two images, and it was experimentally validated using fluorescent beads on a grooved substrate. The technique was then applied to the measurement of chromatic aberration and the true separation between FISH probes. Because there is no need to use a photoactivated protein, this method is applicable to a wide range of fluorescent probes and to nondestructive defect inspection of silicon substrates. The proposed method was composed on the assumption that the fluorescent markers are point sources. Therefore this method is suitable for pinpointing small markers. Because the normal length of FISH probes is 500 kilobase and its size is less than $1.5\,\mu$m, the proposed method is suitable for FISH specimen. On the other hand, there are many shapes and sizes of the defect in silicon substrate. Although the precision of localization is degraded when the defect is not small, the rough localization precision is permissible. In actual case of nondestructive defect inspection of silicon substrate, the precision of localization is required when the small defect is within the top $0.5\,\mu$m of the substrate.

This method uses two exposure steps. In the first, the x and y positions of fluorescent markers are identified using through-focus exposure. In the second step, the z position is identified by analysis of a blurred image taken while moving the specimen along three axes. Using a multiband filter set and a color camera, the method can be applied to measure the distance between fluorescent probes of different colors.

In case the marker images with same colors are closely located or overlapped either in the first or in the second exposure, the localization process in z direction should be modified. The modified localization process will pinpoint the multiple markers by following two steps. First is estimating a number of overlapped markers by analyzing the brightness and shapes of images captured by the first and the second step exposures. Second is localizing the numbers of markers with assuming that there are estimated numbers of markers. By adopting this modification, three dimensional shape and size of the marker will be measured.

With the experimental parameters in this paper, the depth scanning range was $6\,\mu$m with a localization error of less than $0.1\,\mu$m. The effective image capturing area was $714\,\mu\text{m} \times 472\,\mu\text{m}$ and $352\,\mu\text{m} \times 231\,\mu\text{m}$ using a 20× and 40× objective lens, respectively, which corresponds to 96% and 93% of the original image area. We have not completely optimized the parameter of stage movement. The $5\,\mu$m of radius L was decided from the memory capacity of XY stage controller. The stage parameters and the exposure times can be modified if necessary.

The proposed method is fast and requires much less memory for image storage than conventional methods. It is therefore promising as a technique for routinely measuring the separation of fluorescent markers.

Because the depth information for the fluorescent marker is projected onto the xy plane of the imaging device, each marker occupies more pixels than with the traditional method. Therefore, specimens with a high density of markers are less suitable since overlap is likely to occur. However, the method is highly suited to studies of biological specimens such as urine or blood and for defect inspection in semiconductors. With regard to the requirement condition of the specimen in proposed method, the marker is fixed and its brightness is stable during whole process time of 12 s. Considering that the current in vivo imaging using PALM was performed with the exposure time of 25 s [10], an application of proposed method for in vivo imaging might be controversial.

References

1. D. Pinkel, T. Straume, and J. W. Gray, "Cytogenetic analysis using quantitative, high-sensitivity, fluorescence hybridization," Proc. Natl. Acad. Sci. USA **83**, 2934–2938 (1986).
2. D. Pinkel, J. Landegent, C. Collins, J. Fuscoe, R. Segraves, J. Lucas, and J. Gray, "Fluorescence in situ hybridization with human chromosome-specific libraries: Detection of trisomy 21 translocations of chromosome 4," Proc. Natl. Acad. Sci. **85**, 9138–9142 (1988).
3. T. J. Lynch, D. W. Bell, R. Sordella, S. Gurubhagavatula, R. A. Okimoto, B. W. Brannigan, P. L. Harris, S. M. Haserlat, J. G. Supko, F. G. Haluska, D. N. Louis, D. C. Christiani, J. Settleman, and D. A. Haber, "Activating mutations in the epidermal growth factor receptor underlying responsiveness of non–small-cell

lung cancer to Gefitinib," N. Engl. J. Med. **350**, 2129–2139 (2004).
4. M. Uemura, Y. Niwa, N. Kakazu, N. Adachi, and K. Kinoshita, "Chromosomal manipulation by site-specific recombinases and fluorescent protein-based vectors," PLoS One **5**, e9846 (2010).
5. S. W. Hell and J. Wichmann, "Breaking the diffraction resolution limit by stimulated emission: stimulated-emission-depletion fluorescence microscopy," Opt. Lett. **19**, 780–782 (1994).
6. T. A. Klar and S. W. Hell, "Subdiffraction resolution in far-field fluorescence microscopy," Opt. Lett. **24**, 954–956 (1999).
7. R. Heintzmann, T. M. Jovin, and C. Cremer, "Saturated patterned excitation microscopy—a concept for optical resolution improvement," J. Opt. Soc. Am. A **19**, 1599–1609 (2002).
8. E. Betzig, G. H. Patterson, R. Sougrat, O. W. Lindwasser, S. Olenych, J. S. Bonifacino, M. W. Davidson, J. Lippincott, and H. F. Hess, "Imaging intracellular fluorescent proteins at nanometer resolution," Science **313**, 1642–1645 (2006).
9. M. J. Rust, M. Bates, and X. Zhuang, "Sub-diffraction-limit imaging by stochastic optical reconstruction microscopy (STORM)," Nat. Methods **3**, 793–796 (2006).
10. H. Shroff, C. G. Galbraith, J. A. Galbraith, and E. Betzig, "Live-cell photoactivated localization microscopy of nanoscale adhesion dynamics," Nat. Methods **5**, 417–423 (2008).
11. T. Dertinger, R. Colyer, G. Lyer, S. Weiss, and J. Enderlein, "Fast, background-free, 3D super-resolution optical fluctuation imaging (SOFI)," Proc. Natl. Acad. Sci. **106**, 22287–22292 (2009).
12. S. R. P. Pavani, M. A. Thompson, J. S. Biteen, S. J. Lord, N. Liu, R. J. Twieg, R. Piestun, and W. E. Moerner, "Three-dimensional, single-molecule fluorescence imaging beyond the diffraction limit by using a double-helix point spread function," Proc. Natl. Acad. Sci. **106**, 2995–2999 (2009).
13. J. Rosen and G. Brooker, "Non-scanning motionless fluorescence three-dimensional holographic microscopy," Nat. Photonics **2**, 190–195 (2008).
14. C. Maurer, S. Khan, S. Fassl, S. Bernet, and M. Ritsch-Marte, "Depth of field multiplexing in microscopy," Opt. Express **18**, 3023–3033 (2010).
15. L. Holtzer, T. Meckel, and T. Schmidt, "Nanometric three-dimensional tracking of individual quantum dots in cells," Appl. Phys. Lett. **90**, 053902 (2007).
16. P. A. Dalgarno, H. I. C. Dalgarno, A. Putoud, R. Lambert, L. Paterson, D. C. Logan, D. P. Towers, R. J. Warburton, and A. H. Greenaway, "Multiplane imaging and three dimensional nanoscale particle tracking in biological microscopy," Opt. Express **18**, 877–883 (2010).
17. W. A. Nevin, D. L. Gay, and V. Higgs, "Photoluminescence study of interfacial defects in direct-bonded silicon wafers," J. Electrochem. Soc. **150**, G591–G596 (2003).
18. C. Gunn, "CMOS photonics for high-speed interconnects," Micro. IEEE **26**, 58–66 (2005).
19. L. Liao, D. Samara-Rubio, M. Morse, A. Liu, D. Hodge, D. Rubin, U. Keil, and T. Franck, "High speed silicon Mach–Zehnder modulator," Opt. Express **13**, 3129 (2005).
20. T. Indukuri, P. Koonath, and B. Jalali, "Three-dimensional integration of metal-oxide-semiconductor transistor with subterranean photonics in silicon," Appl. Phys. Lett. **88**, 121108 (2006).
21. K. Kishima, "Analysis of defects in an electric and photonic double-layer substrate made by separation-by-implanted-oxygen three-dimensional sculpting," Appl. Phys. Lett. **89**, 201109 (2006).
22. E. R. Dowski, Jr., and W. T. Cathey, "Extended depth of field through wave-front coding," Appl. Opt. **34**, 1859–1866 (1995).
23. A. Veeraraghavan, R. Raskar, A. Agrawal, A. Mohan, and J. Tumblin, "Dappled photography: Mask enhanced cameras for heterodyned light fields and coded aperture refocusing," ACM Trans. Graphics **26**, 69-1–69-12 (2007).
24. M. Levoy, R. Ng, A. Adams, M. Footer, and M. Horowitz, "Light field microscopy," ACM Trans. Graphics **25**, 924–934 (2006).
25. H. Nagahara, S. Kuthirummal, C. Zhou, and S. K. Nayar, "Flexible depth of field photography," in *Proceedings of European Conference on Computer Vision (ECCV)* (Springer-Verlag, 2008), pp. 60–73.
26. J. W. Goodman, *Introduction to Fourier Optics* (Roberts, 2004).
27. http://www.abbottmolecular.com/UroVysion_5181.aspx.
28. http://www.atcc.org/ATCCAdvancedCatalogSearch/ProductDetails/tabid/452/Default.aspx?ATCCNum=CCL-171&Template=cellBiology.